



Can whole-tumor radiomics-based CT analysis better differentiate fat-poor angiomyolipoma from clear cell renal cell carcinoma: compared with conventional CT analysis?

Yanqing Ma¹ · Fang Cao¹ · Xiren Xu¹ · Weijun Ma²

Published online: 24 January 2020

© Springer Science+Business Media, LLC, part of Springer Nature 2020

Abstract

Purpose This study aimed to discriminate fat-poor angiomyolipoma (fp-AML) from clear cell renal cell carcinoma (ccRCC) by constructing radiomics-based logistic classifiers in comparison with conventional computed tomography (CT) analysis at three CT phases.

Materials and methods Twenty-two fp-AML patients and 62 ccRCC patients who were pathologically identified were enrolled in this study, and underwent three-phase (unenanced phase, UP; corticomedullary phase, CMP; nephrographic phase, NP) CT examinations. Whole-tumor regions of interest (ROIs) were contoured in ITK software by two radiologists. Radiomic features were dimensionally reduced by means of ANOVA+MW, correlation analysis, and LASSO. Four radiomics logistic classifiers including the UP group, CMP group, NP group, and sum group were built, and the radiomic scores (rad-scores) were calculated. After collecting the qualitative and quantitative conventional CT characteristics, the conventional CT analysis logistic classifier and the radiomics-based logistic classifier were constructed. The receiver operating characteristic curve (ROC) was constructed to evaluate the validity of each classifier.

Results The area under curve (AUC) of the conventional CT analysis logistic classifier including angular interface, cyst degeneration, and pseudocapsule was 0.935 (95% CI 0.860–0.977). Regarding logistic classifiers for radiomics analysis, the AUCs of the UP group were 0.950 (95% CI 0.895–1.000) and 0.917 (95% CI 0.801–1.000) in the training set and testing set, respectively, which were higher than those of the CMP and NP groups. The AUCs of the sum group were observed to be the highest. The top three selected features for the UP and sum groups belonged to GLCM parameters and histogram parameters. The radiomics-based logistic classifier encompassed cyst degeneration, pseudocapsule, and sum rad-score, and the AUC of the model was 0.988 (95% CI 0.935–1.000).

Conclusion Whole-tumor radiomics-based CT analysis is superior to conventional CT analysis in the differentiation of fp-AML from ccRCC. Cyst degeneration, pseudocapsule, and sum rad-score are the most significant factors. The radiomics analysis of the UP group shows a higher AUC than that of the CMP and NP groups.

Keywords Angiomyolipoma · Clear cell renal cell carcinoma · Radiomics · Computed tomography

✉ Yanqing Ma
704180026@qq.com

Fang Cao
Caofangry1988@163.com

Xiren Xu
Xuxiren1966@163.com

Weijun Ma
Maweijun1985@163.com

¹ Department of Radiology, Zhejiang Provincial People's Hospital, People's Hospital of Hangzhou Medical College, 310000 Hangzhou, China

² Department of Neurosurgery, Shaoxing City Keqiao District Hospital of Traditional Chinese Medicine, 312000 Shaoxing, China

Introduction

AML is a member of perivascular epithelioid cell tumors (PEComas) [1], which is composed of varying amounts of dysmorphic blood tissue, smooth muscle components, and mature adipose tissue [2]. It is the most common benign solid renal neoplasm [2]. Macroscopic fat may be easily detected in most AML patients on computed tomography (CT), or magnetic resonance imaging (MRI) [3]. However, up to 5% of renal AMLs lack macroscopic fat [4], making these lesions controversial to differentiate from renal cancer in conventional CT analysis [5]. Fp-AML is defined as an angiomyolipoma containing little to no fat. It is most commonly encountered in the 4th to 6th decades of life, exhibiting female preponderance [6]. Terms like “angiomyolipoma without visible fat” [7], “angiomyolipoma with minimal fat” [8], and “lipid-poor angiomyolipoma” [9] have been used in previous studies to describe this condition. To deter confusion and potential errors, the term “fat-poor angiomyolipoma” was denominated to chosen.

Varieties of studies have been investigated the differentiation of fp-AML from ccRCC via CT images. Kim et al. [10] showed that fp-AML tends to be hyperattenuating, has an angular interface on unenhanced CT and possesses a homogeneous, prolonged enhancement on enhanced CT. However, other studies have stated that these CT findings are non-specific, and that both fp-AML and ccRCC patients present with heterogeneous enhancement [11]. Yan et al. [8] believed that multi-phase CT scanning may be able to distinguish between fp-AML, papillary RCC, and ccRCC. The enhancement degree of fp-AML varies according to the number of vessels, and is sometimes similar to that of ccRCC. It is the visual similarity of substantial overlapping characteristics between two diseases that makes it imperative to differentiate.

Radiomics, a newly emerging computer-assisted technique, converts the conventional visual images into large amounts of quantitative features [12]. These features cover voxel intensity, three-dimensional shape and size, appearance of surface, and gray-level co-occurrence. Feng et al. [13] have pointed out that machine learning-based quantitative texture analysis may facilitate the accurate differentiation of fp-AML from renal cell carcinoma (RCC). However, CT texture analysis presents lower lesion homogeneity and higher lesion entropy in RCCs than in fp-AMLs on unenhanced CT images [14]. One study has demonstrated that single/selected-slice ROI texture analysis may help differentiate fp-AML from RCC [12]. Though, radiomic features of the lesions may cover the data obtained from conventional CT analysis. The inconsistent expression and varied repeatability make such a comparison necessary. Therefore, diagnosis using

conventional CT analysis along with the help of radiomics analysis may provide advantages in differentiating fp-AML from ccRCC.

To the best of our knowledge, no study has compared the differentiation of the two maladies between conventional CT analysis and radiomics-based CT analysis. Therefore, this study puts forward the construction of a whole-tumor radiomics-based logistic classifier to better differentiate fp-AML from ccRCC in CT imaging.

Materials and methods

Patient acquisition

This retrospective study was approved by the institutional review board. For this type of study, formal written consent was not required.

All data were collected from the Picture Archiving and Communication System (PACS) database from January 2014 to January 2019. There were 534 patients diagnosed as renal masses or suspected renal tumors. The inclusion criteria of this study were as follows: (1) All patients underwent three-phase CT scan (UP, CMP and NP) with the same CT protocols. (2) Their diagnosis were histopathologically confirmed by partial or total surgical resection. (3) There was no visible macroscopic fat within the renal masses on unenhanced CT images, diagnosed by two radiologists. (4) All patients were found to harbor primarily solid lesions, without hemorrhage, or large fluid collection. Finally, our cohort involved 22 fp-AML patients, and 62 ccRCC patients (Fig. 1).

CT examination

All examinations were performed using 64/128-slice multi-detector CT (SOMATOM Definition AS, Siemens Healthcare). By the computer-assisted bolus-tracking technology, scan delays were 15 s and 30 s for the CMP and NP, respectively, with a 100-Hu threshold in the abdominal aorta at the level of the celiac artery as the baseline. Patients received 90–100 milliliters of contrast material (Iopromide, 370), which was administered into an antecubital vein with a power injector at a rate of 3.0 mL/s. The scanning parameters were as follows: tube voltage, 120 kV; tube current, 200 mA; collimation, 64 × 0.625 mm; rotation time, 0.75 s; pitch, 1.375:1; and field of view, 360 mm.

Conventional CT analysis

Two radiologists with 10-year and 7-year CT diagnostic experience analyzed all of the images, respectively.

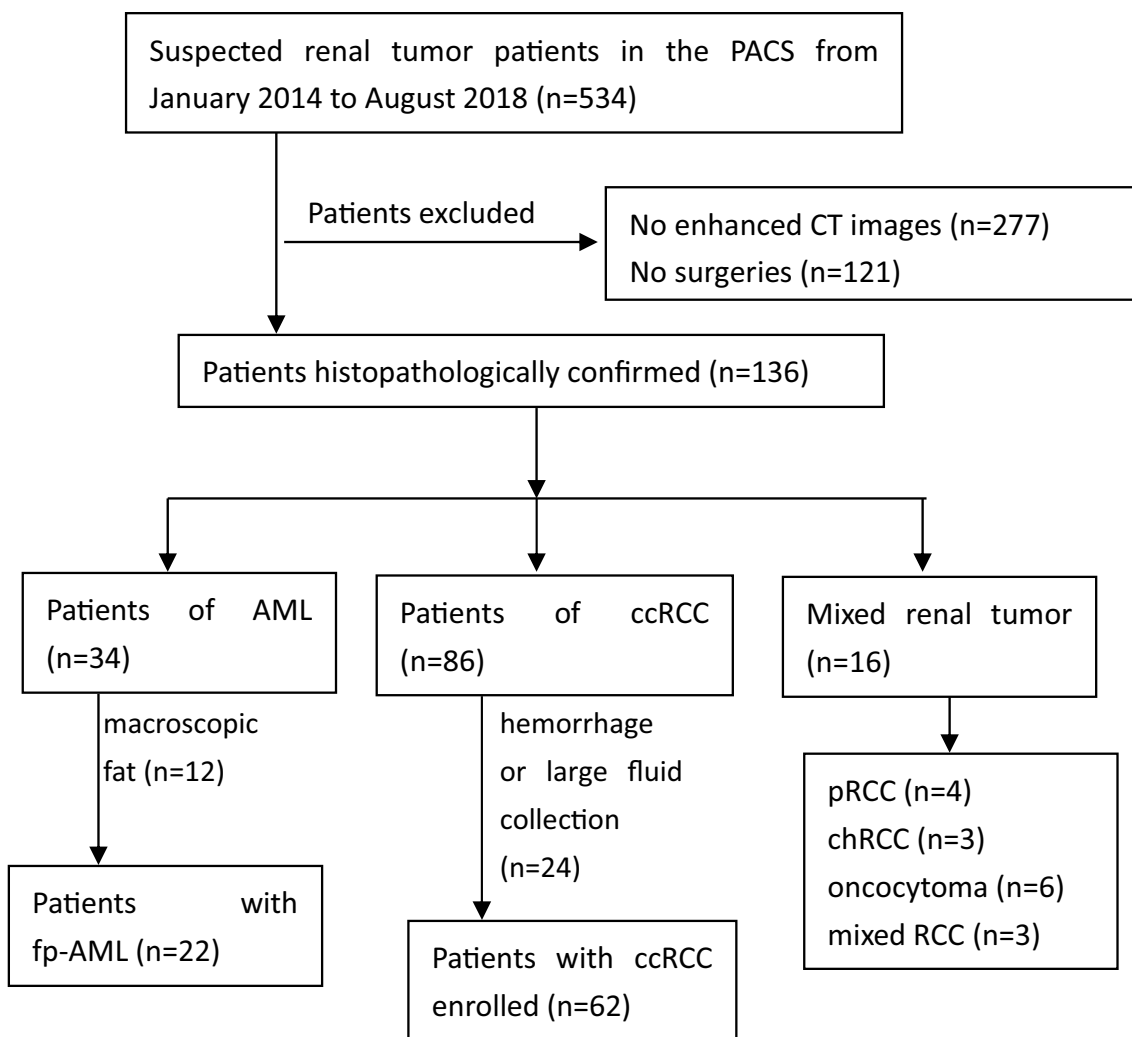


Fig. 1 *pRCC* papillary renal cell carcinoma; *chRCC* chromophobe renal cell carcinoma; *mixed RCC* included renal collecting duct carcinoma, and neuroendocrine tumor

Eventually, the data were recorded upon reaching a final decision after consensus or adjudication by two radiologists.

Conventional qualitative CT features of location (left/right), growth pattern (exophytic, endophytic), angular interface (pyramidal, interface with a definable apex within the parenchyma and an exophytic bulging of the mass beyond the renal capsule [7], Fig. 2a), cyst degeneration, calcification, pseudocapsule (pathologically, a fibrous tissue that compressed renal mass, showing the high-attenuation rim around the mass on contrast-enhanced CT images [7], Fig. 2b), enhancement pattern (homogeneous, heterogeneous), and gender were analyzed (Table 1).

Conventional quantitative CT features including size, UP CT value (UP renal mass CT value), CMP-enhanced CT value (calculated as: CMP renal mass CT value – UP renal mass CT value), CMP/renal% (defined as: CMP-enhanced CT value/renal parenchyma CT value \times 100%), NP-enhanced

CT value (calculated as: NP renal mass CT value – CMP renal mass CT value), NP/renal% (estimated as: NP-enhanced CT value/renal parenchyma CT value \times 100%), and age were calculated (Table 1). To reduce attenuation variation due to individual patient and examination technology, relative renal mass CT value was obtained. The relative lesion CT value was normalized by renal parenchyma attenuation.

Image segmentation and features selection

The slice thickness for all three-phase images was 5 mm, with the window width and level were 300 Hu and 40 Hu. The manual defined smooth curve ROI was delineated slightly smaller in size than the actual tumor size, maintaining an approximate 2–3 mm distance from the tumor margin, to minimize the partial volume effect from surrounding renal

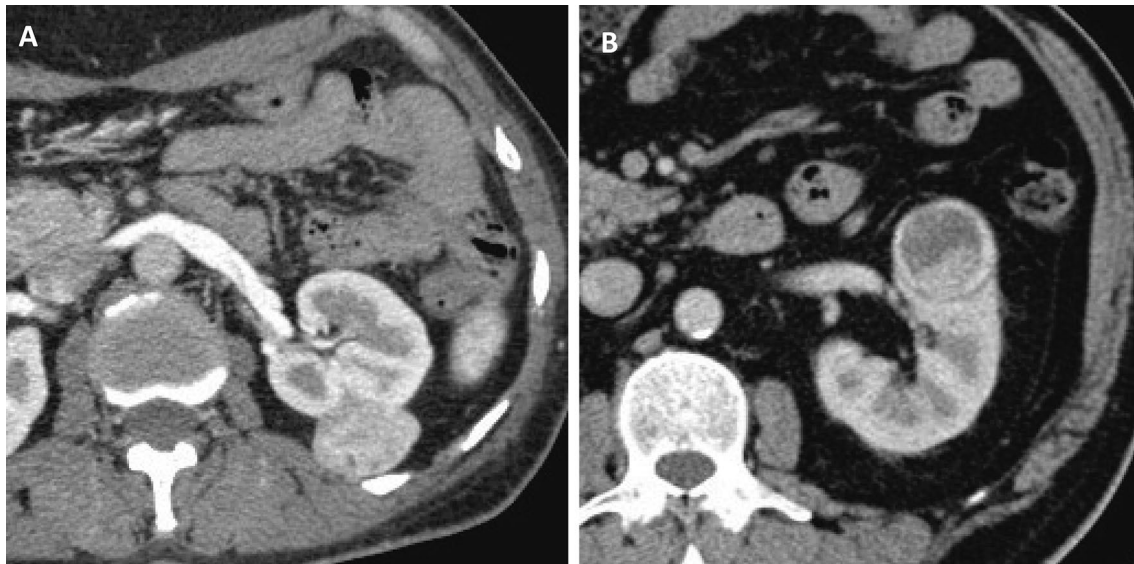


Fig. 2 **a** Exhibited the sign of imageangular interface, showing the pyramidal interface within the parenchyma and an exophytic bulging of the mass beyond the renal capsule. **b** Exhibited the sign of pseudo-

capsule, showing the high-attenuation rim around the mass on contrast-enhanced CT images

Table 1 Data of Conventional CT analysis

Conventional CT features	ccRCC	fp-AML	<i>p</i> value
Gender (female/male)	24 (38.7%)/38 (61.3%)	16 (72.7%)/6 (27.3%)	0.070
Age	57.9 ± 10.8	50.5 ± 12.8	0.010
Size	37.4 ± 15.6	32.0 ± 9.8	0.065
Location (left/right)	28 (45.2%)/34 (54.8%)	8 (36.4%)/14 (63.6%)	0.617
Growth pattern (exophytic/endophytic)	28 (45.2%)/34 (54.8%)	9 (40.9%)/13 (59.1%)	0.806
Angular interface	2(3.2%)	14 (63.6%)	0.000
Cyst degeneration	38 (61.3%)	2 (9.1%)	0.000
Calcification	8 (12.9%)	1 (4.5%)	0.434
Pseudocapsule	38 (61.3%)	1 (4.5%)	0.000
Enhancement pattern (homogeneous/heterogeneous)	20 (32.3%)/42 (67.7%)	14 (63.6%)/8 (36.4%)	0.321
UP CT value	75.5 ± 20.4	91.8 ± 11.3	0.000
CMP-enhanced CT value	85.3 ± 34.8	69.2 ± 35.9	0.079
CMP/renal%	64.3 ± 23.8	50.1 ± 22.5	0.024
NP-enhanced CT value	28.9 ± 22.2	20.4 ± 17.6	0.352
NP/renal%	23.6 ± 20.6	12.9 ± 10.8	0.012

The conventional qualitative CT features, including gender, location, growth pattern, angular interface, cyst degeneration, calcification, pseudocapsule, enhancement pattern, were compared using method of Chi-square test in SPSS. The conventional quantitative CT features including age, size, UP CT value, CMP-enhanced CT value, CMP/renal%, NP-enhanced CT value, NP/renal%, were compared with method of independent *t* test

p < 0.05 Showed significant difference

parenchyma and perinephric fat (Fig. 3a, b). Whole-tumor ROIs were constructed using all slice images except for the first and last ones. After offering the corresponding contrast CT images, the margin of the mass at UP was defined. The ROIs were depicted in the software “ITK-SNAP” Version 3.4.0 (<http://www.itksnap.org/>).

Radiomics features referring to histogram parameters, texture parameters, form factor parameters, GLCM parameters, and RLM parameters, were calculated by AK software (Artificial Intelligence Kit, Version 3.0.0, GE Healthcare). A totally of 396 features were extracted by three steps: Firstly, it replaced the abnormal values by mean to standardize

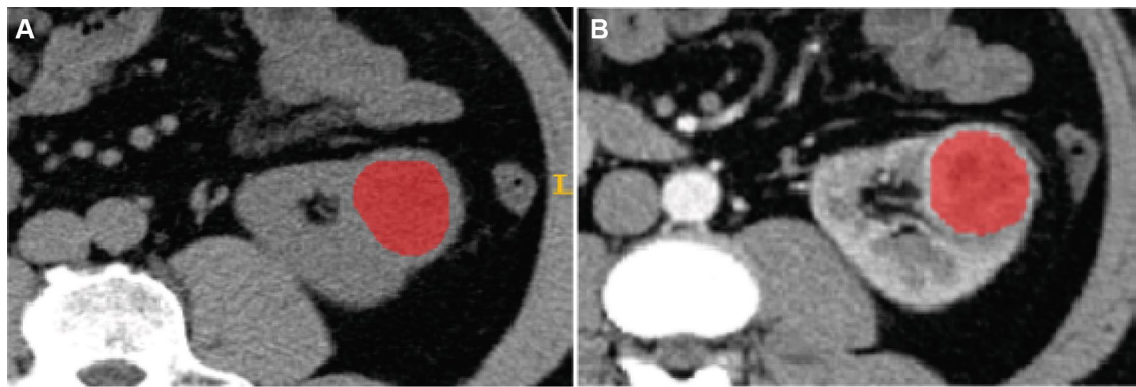


Fig. 3 The lesion contour at unenhanced phase (a) was guided by the corresponding contrast-enhanced CT image (b). Manual defined smooth curve ROIs were delineated maintaining a 2–3 mm distance from the tumor margin

the data, which could remove the unit limits of the data. Secondly, it partitioned the training set and testing set with a proportion of 7:3. Thirdly, by the methods of variance (ANOVA), Mann–Whitney *U* test (MW), the correlation test, and the Least Absolute Shrinkage and Selection Operator (LASSO), the features were further extracted to reduce the redundant dimensions.

Conventional CT analysis and radiomics-based logistic classifiers construction

Four simple radiomics logistic classifiers including the UP group, CMP group, NP group, and sum group models were constructed to evaluate the radiomics diagnostic accuracy at different phases. And rad-scores including the UP rad-score, CMP rad-score, NP rad-score, and sum rad-score of every patient at different phases were calculated. The conventional CT analysis logistic classifier including qualitative and quantitative CT features was constructed. The sum rad-score as a radiomic factor was used to construct a radiomics-based logistic classifier, which also included the conventional CT features. The AUCs of ROC curve in the training set and testing set were calculated to evaluate the predictive accuracy of the different logistic classifiers.

Statistical analysis

The ANOVA + MW, correlation analysis, and LASSO statistical analysis were performed using R software (version 3.6.1). The four simple radiomics logistic classifiers (UP group, CMP group, NP group, sum group models) and the rad-scores were also constructed and analyzed by R software. The significant set was 0.05. The Chi-square test, independent *t* test, and multivariate logistic regression were performed by SPSS (IBM Statistics SPSS 22.0). A *p* value of <0.05 was considered as statistically significant. The conventional CT qualitative and quantitative features

were analyzed by Chi-square test or independent *t* test, and the features with *p* < 0.05 were considered as candidate factors in a multivariate logistic model. The comparative ROC curve of the conventional CT analysis and radiomics-based analysis was performed by MedCalc. The intra-class correlation coefficient (ICC) was used to evaluate the intra-observer agreement.

Results

Conventional qualitative and quantitative CT analysis

In this cohort, 22 fp-AML patients (including, 72.7% of females with a mean age of 50.5 ± 12.8 years) and 62 ccRCC patients (including, 38.7% of females with a mean age of 57.9 ± 10.8 years) were enrolled. There was no statistical significance in some qualitative variables (gender, location, growth pattern, calcification, and enhancement pattern) as well as certain quantitative variables (size, CMP-enhanced CT value, and NP-enhanced CT value). The variables including angular interface (*p* = 0.000), cyst degeneration (*p* = 0.000), pseudocapsule (*p* = 0.000), age (*p* = 0.010), UP CT value (*p* = 0.000), CMP/renal% (*p* = 0.024), and NP/renal% (*p* = 0.012) demonstrated statistical significance and were selected as independent predictors to construct conventional CT analysis logistic model (Table 1). Angular interface, cyst degeneration, and pseudocapsule were determined to be the final optimal features in the logistic classifier. The AUC of the conventional CT analysis model was 0.935 (95% CI 0.860–0.977).

Radiomics analysis

Four single radiomics analysis logistic classifiers, namely the UP group, CMP group, NP group and sum group, were

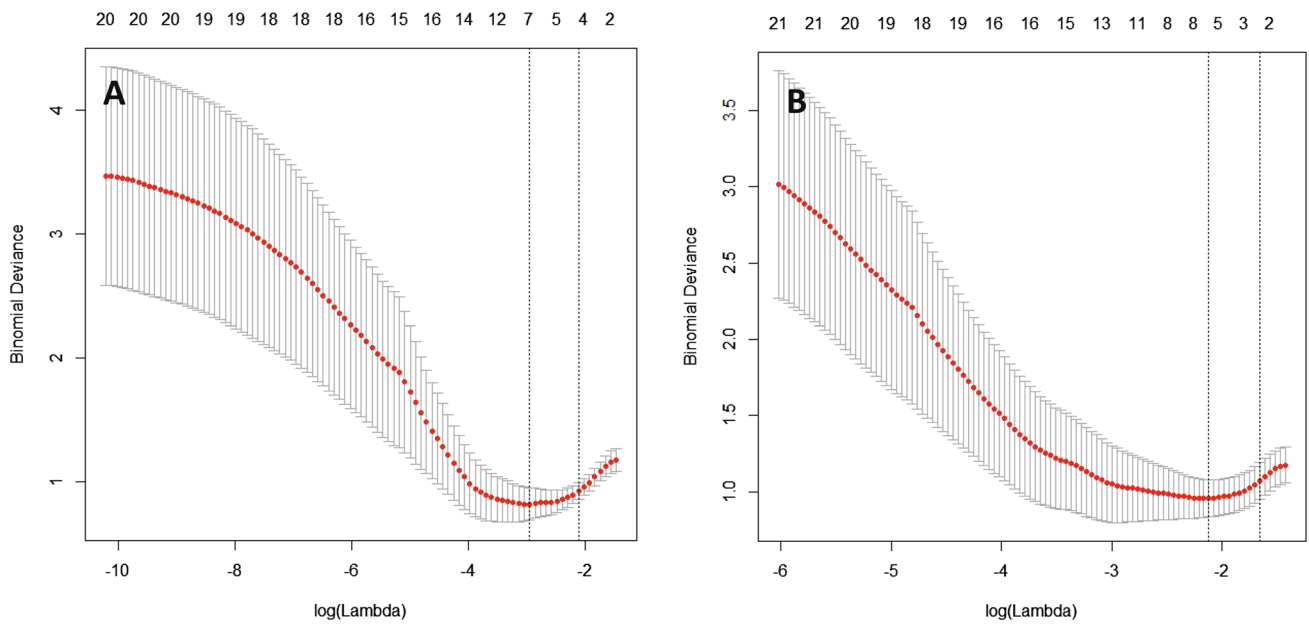


Fig. 4 Plot of LASSO coefficients-lambda for the UP group (a) and sum group (b). Ten fold cross-validation via minimum criteria was used in the LASSO model. The dotted vertical lines were drawn

taking the optimal values, seven and six features were eventually selected for the UP group and sum group

Table 2 The diagnosis of simple radiomic classifiers

Logistic classifier	AUC of training set	95% CI	AUC of testing set	95% CI
UP group model	0.950	0.895–1.000	0.917	0.801–1.000
CMP group model	0.839	0.710–0.967	0.827	0.662–0.992
NP group model	0.840	0.735–0.946	0.865	0.723–1.000
Sum group model	0.964	0.915–1.000	0.925	0.824–1.000

constructed, respectively. The UP group finally included seven optimal features with AUCs of 0.950 (95% CI 0.895–1.000) and 0.917 (95% CI 0.801–1.000) in the training set and testing set (Fig. 4a). In regard to the CMP group, six optimal features were involved, with AUCs of 0.839 (95% CI 0.710–0.967) and 0.827 (95% CI 0.662–0.992) in the training set and testing set. The NP group finally contained 3 optimal features with AUCs of 0.840 (95% CI 0.735–0.946) and 0.865 (95% CI 0.723–1.000) in the two sets. Six optimal features were finally remained in the sum group (Fig. 4b), with the corresponding AUCs of 0.964 (95% CI 0.915–1.000) and 0.925 (95% CI 0.824–1.000) in the two sets (Table 2). The AUC of the UP group was larger than that of either the CMP group or the NP group, while the AUC of the sum group was observed to be the largest.

The radiomics-based logistic model was constructed and encompassed the factors of angular interface, cyst

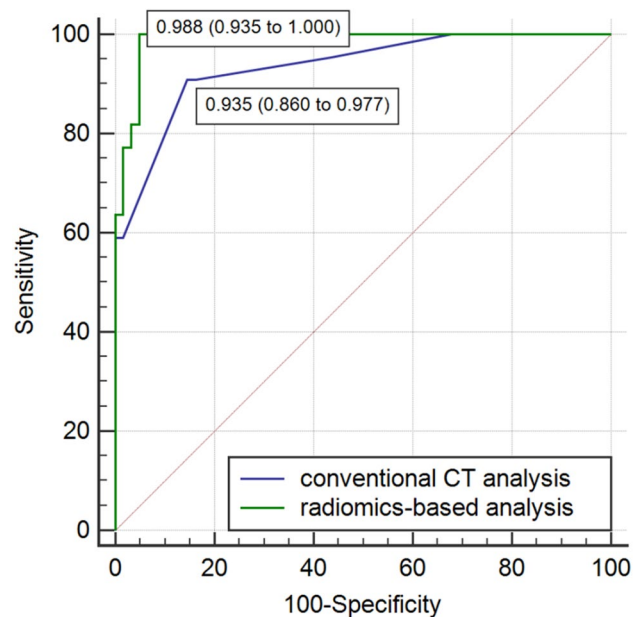


Fig. 5 ROC curve of conventional CT analysis and radiomics-based analysis. The AUCs were 0.935 (95% CI 0.860 to 0.977) and 0.988 (95% CI 0.935 to 1.000), respectively

degeneration, pseudocapsule, age, UP CT value, CMP/renal%, NP/renal%, and sum rad-scores. The AUC of this model was 0.988 (95% CI 0.935–1.000), which was slightly higher than 0.935 (95% CI 0.860–0.977) of the conventional CT analysis mode, but shared a overlapping 95% CI (Fig. 5).

The intra-observer agreement

Two radiologists with 10-years and 7-years CT diagnostic experience delineated the ROIs and collected the conventional CT features, respectively. We compared the data of the extracted radiomics features in the sum group and the conventional CT features collected by two radiologists, and the ICC was found to be 0.796 to 0.939. An ICC greater than 0.75 was considered to be of good agreement.

Discussion

Conventional CT analysis has provided useful information regarding the differentiation between fp-AML and ccRCC. In this study, the angular interface, cyst degeneration, and pseudocapsule were determined to be the final optimal features among conventional CT analysis logistic classifier. The ccRCC lesions are more vulnerable to be accompanied by cyst degeneration and pseudocapsule, while fp-AML lesions often present with a sign of angular interface. Furthermore, the lesion shape may help to differentiate fp-AML from ccRCC. The angular interface indicates the angular configuration of the parenchymal portions of a tumor [15]. The absence of pseudocapsule is another significant characteristics of fp-AML [8]. Pseudocapsule is composed of fibrous tissue and compressed renal parenchyma, which was seen in 66% of RCC with a diameter of no larger than 4 cm [16].

Compared with the CMP and NP groups, the UP group radiomics model showed a higher AUC. This diverseness illuminates that UP plays a predominant role in distinguishing between two diseases, which aligns with the findings of previous studies. However, the CMP radiomics model, as Shu et al. [17] pointed out, showed the least amount of accuracy in differentiating Fuhrman grades of ccRCC. These corresponding outcomes emphasize the importance of the unenhanced CT scan. While, the degree of enhancement in fp-AML is susceptible to the number of blood vessels in a lesion in an enhanced study. Nonetheless, a part of the explanation may lie in the different scan time. Moreover, there is no standard or consensus on the corresponding CT scan protocols due to the plethora of available scanning technologies, machines, and so forth. A study have directly took 25-s and 70-s delay after contrast injection at CMP and NP [17], while another study have took 30-s and 65 to 70-s delay [18]. Unlike in previous studies, this study adopted the technology of computer-assisted bolus-tracking, and selected 15-s and 30-s delay with a 100-Hu threshold in the abdominal aorta in the CMP and NP. The result pertaining to feature selection for UP group model revealed that the Entropy of GLCM parameters (GLCMEntropy_AllDirection_offset7_SD), haralick features (HaralickCorrelation_angle90_offset7), and histogram parameters (root mean square, RMS) were

the top three ranked parameters. Compared with ccRCC, fp-AML was characterized by a higher Entropy, which may significantly reflect the tumor invasiveness and heterogeneity as previously proven. Haralick features are calculated from the GLCM and are defined as a two dimensional (2D) histogram of pixel gray level, by counting the co-occurrence of neighboring gray levels in images [19].

In this study, the AUC of the sum group was the highest, and the entire diagnostic accuracy in enhanced CT was better than that of unenhanced CT examination. The result of feature selection for the sum group model revealed that the GLCM parameters (Correlation_AllDirection_offset4_SD), histogram parameters (root mean square, RMS), and haralick features (HaralickCorrelation_angle90_offset7) to be the top three parameters. The correlation of GLCM measures the similarity of the gray levels in neighboring pixels, reflecting how correlated a pixel is with its neighbor throughout the whole image.

Percutaneous biopsy has been prevalent in pathological diagnosis, though it is attributed with a 10–20% non-diagnostic rate [20]. However, radiological diagnosis still takes an important role in differentiating fp-AML from ccRCC. The radiomics-based logistic classifier may improve the accuracy of differentiation to 0.988 from 0.935 of the conventional CT analysis logistic classifier. Thus, this novel and non-invasive biomarker may help better differentiate the two diseases. However, a comparison between pathological biopsy and diagnostic CT features among the same cohort remains further study. So far, a number of studies have involved the application of machine-based quantitative analyses in differentiating fp-AML from ccRCC [2, 12], though most of them are confined to histogram or texture analysis [12]. Performing a histogram analysis as first order statistics depicts the most intuitive image features in application. It only reflects the distribution of gray level but ignores the spatial interaction between pixels. However, whether the whole-tumor analysis is superior to the 2-dimensional analysis remains a moot point [17]. Hotker et al. [20] discovered that whole-tumor analysis demonstrates better inter-observer agreement and lower variability. Moreover, Feng et al. [13] have uncovered that whole-tumor analysis appears to be more indicative in evaluating tumor heterogeneity than a 2-dimensional analysis. In this study, radiomics analysis was quantified in detail, with a total of 396 features (e.g., histogram parameters, texture parameters, form factor parameters, GLCM parameters, and RLM parameters) offered for further selection using statistical methods. Furthermore, the rad-score was computed, which expressed all the radiomics parameters, and elevated the AUC from 0.935 to 0.988, compared with the conventional CT analysis. The angular interface, cyst degeneration, and sum rad-score were observed to be independent factors according to radiomics-based logistic regression when differentiating fp-AML from ccRCC.

Besides, there are several limitations in the present study. Firstly, the total sample size of this study is small, because many patients with a correct diagnosis of fp-AML were suggested to follow-up without surgery and were thus excluded from the study. Secondly, owing to the insufficient sample size, the Fuhrman classification in ccRCC group was limited. Thirdly, the data of two groups may not identically match in size, gender, and age. Hence, a multicentric trial employing a larger samples size is essential in diminishing the differences between the groups.

Conclusions

Radiomics-based analysis may better differentiate fp-AML from ccRCC in three CT phases. The angular interface, cyst degeneration, and sum rad-score are independent factors for the radiomics-based logistic classifier. The AUC of the UP radiomics logistic classifier is higher than that of the CMP and NP logistic classifier, which accentuates the importance of UP. The selected features from the histogram parameters and GLCM parameters may be potential radiomic biomarkers for distinguishing between the fat-poor angiomyolipoma and clear cell renal cell carcinoma.

Compliance with ethical standards

Conflict of interest The authors declare that they have no conflict of interest.

References

- Jinzaki M, Silverman S G, Akita H, et al., Renal angiomyolipoma: a radiological classification and update on recent developments in diagnosis and management[J]. *Abdominal Imaging*, 2014, 39(3):588-604.
- Taryn H, Mcinnes M D F, Nicola S, et al., Can Quantitative CT Texture Analysis be Used to Differentiate Fat-poor Renal Angiomyolipoma from Renal Cell Carcinoma on Unenhanced CT Images?[J]. *Radiology*, 2015, 276(3):787-96.
- Park B K, Renal Angiomyolipoma: Radiologic Classification and Imaging Features According to the Amount of Fat[J]. *AJR Am J Roentgenol*, 2017, 209(4):1-10.
- Wasser E J, Shyn P B, Riveros-Angel M, et al., Renal cell carcinoma containing abundant non-calcified fat[J]. *Abdominal Imaging*, 2013, 38(3):598-602.
- Kim R, Lee J M, Joo I, et al., Differentiation of lipid poor angiomyolipoma from hepatocellular carcinoma on gadoteric acid-enhanced liver MR imaging[J]. *Abdominal Imaging*, 2015, 40(3):531-41.
- Sureka B, Khera P S, Radiologic Classification and Imaging Features of Renal Angiomyolipomas According to the Amount of Fat[J]. *Ajr American Journal of Roentgenology*, 2018, 210(3):W136-W136.
- Lee H, Hong H, Kim J, et al., Deep Feature Classification of Angiomyolipoma without Visible Fat and Renal Cell Carcinoma in Abdominal Contrast-Enhanced CT Images with Texture Image Patches and Hand-Crafted Feature Concatenation[J]. *Medical Physics*, 2018, 45(4):1550-1561.
- Yan L, Liu Z, Wang G, et al., Angiomyolipoma with minimal fat: differentiation from clear cell renal cell carcinoma and papillary renal cell carcinoma by texture analysis on CT images[J]. *Academic Radiology*, 2015, 22(9):1115-1121.
- Ishigami K, Pakalniskis M G, Leite L V, et al., Characterization of renal cell carcinoma, oncocytoma, and lipid-poor angiomyolipoma by unenhanced, nephrographic, and delayed phase contrast-enhanced computed tomography[J]. *Clin Imaging*, 2015, 39(1):76-84.
- Kim S H, Kim C S, Kim M J, et al., Differentiation of Clear Cell Renal Cell Carcinoma From Other Subtypes and Fat-Poor Angiomyolipoma by Use of Quantitative Enhancement Measurement During Three-Phase MDCT[J]. *Ajr American Journal of Roentgenology*, 2015, 206(1):W21.
- Takahashi N, Leng S, Kitajima K, et al., Small (< 4 cm) Renal Masses: Differentiation of Angiomyolipoma Without Visible Fat From Renal Cell Carcinoma Using Unenhanced and Contrast-Enhanced CT[J]. *Ajr American Journal of Roentgenology*, 2015, 205(6):1194-202.
- Li H, Li A, Hui Z, et al., Whole-Tumor Quantitative Apparent Diffusion Coefficient Histogram and Texture Analysis to Differentiation of Minimal Fat Angiomyolipoma from Clear Cell Renal Cell Carcinoma[J]. *Academic Radiology*, 2018, S1076633218303295-.
- Feng Z, Rong P, Cao P, et al., Machine learning-based quantitative texture analysis of CT images of small renal masses: Differentiation of angiomyolipoma without visible fat from renal cell carcinoma[J]. *Eur Radiol*, 2018, 28(4):1625-1633.
- Sasiwimonphan K, Takahashi N, Leibovich B C, et al., Small (< 4 cm) renal mass: differentiation of angiomyolipoma without visible fat from renal cell carcinoma utilizing MR imaging[J]. *Radiology*, 2012, 263(1):160.
- Farber N J, Wu Y, Zou L, et al., Challenges in RCC Imaging: Renal Insufficiency, Post-Operative Surveillance, and the Role of Radiomics[J]. *Kidney Cancer Journal Official Journal of the Kidney Cancer Association*, 2015, 13(4):84.
- Yamashita Y, Honda S, Nishiharu T, et al., Detection of pseudocapsule of renal cell carcinoma with MR imaging and CT[J]. *AJR Am J Roentgenol*, 1996, 166(5):1151-1155.
- Shu J, Tang Y, Cui J, et al., Clear cell renal cell carcinoma: CT-based radiomics features for the prediction of Fuhrman Grade[J]. *European Journal of Radiology*, 2018, 109).
- Li Z C, Zhai G, Zhang J, et al., Differentiation of clear cell and non-clear cell renal cell carcinomas by all-relevant radiomics features from multiphase CT: a VHL mutation perspective[J]. *Eur Radiol*, 2018.
- Delgado A F, Fahlström M, Nilsson M, et al., Diffusion Kurtosis Imaging of Gliomas Grades II and III - A Study of Perilesional Tumor Infiltration, Tumor Grades and Subtypes at Clinical Presentation[J]. *Radiology & Oncology*, 2017, 51(2):121-129.
- Hotker A M, Yousef M, Andreas W, et al., Use of DWI in the Differentiation of Renal Cortical Tumors[J]. *Ajr American Journal of Roentgenology*, 2016, 206(1):100.

Publisher's Note Springer Nature remains neutral with regard to jurisdictional claims in published maps and institutional affiliations.